PCCP

PAPER

View Article Online
View Journal | View Issue

Cite this: *Phys. Chem. Chem. Phys.*, 2015, **17**, 22304

Control of layer stacking in CVD graphene under quasi-static condition

Kiran M. Subhedar,* Indu Sharma and Sanjay R. Dhakate

Received 19th June 2015,
Accepted 27th July 2015

DOI: 10.1039/c5cp03541d

www.rsc.org/pccp

The type of layer stacking in bilayer graphene has a significant influence on its electronic properties because of the contrast nature of layer coupling. Herein, different geometries of the reaction site for the growth of bilayer graphene by the chemical vapor deposition (CVD) technique and their effects on the nature of layer stacking are investigated. Micro-Raman mapping and curve fitting analysis confirmed the type of layer stacking for the CVD grown bilayer graphene. The samples grown with sandwiched structure such as quartz/Cu foil/quartz along with a spacer, between the two quartz plates to create a sealed space, resulted in Bernal or AB stacked bilayer graphene while the sample sandwiched without a spacer produced the twisted bilayer graphene. The contrast difference in the layer stacking is a consequence of the difference in the growth mechanism associated with different geometries of the reaction site. The diffusion dominated process under quasi-static control is responsible for the growth of twisted bilayer graphene in sandwiched geometry while surface controlled growth with ample and continual supply of carbon in sandwiched geometry along with a spacer, leads to AB stacked bilayer graphene. Through this new approach, an efficient technique is presented to control the nature of layer stacking.

Introduction

Since its discovery, single layer graphene has been intriguing the scientific community with its extraordinary properties.[1–5] The possibility of the growth of single layer graphene (SLG) using the thermal chemical vapor deposition (CVD) technique became a paradigm for high quality graphene synthesis, which offers viable technology for wafer scale production of graphene.[6] Apart from SLG, CVD growth can yield bilayer graphene (BLG) or few layer graphene (FLG) with two types of layer stacking; first, AB or Bernal stacking, which is commonly present in graphite and the second one is twisted stacking, where the individual graphene layers are rotationally stacked with some angle. Both types are equally important from the application point of view. The former shows the opening of tunable energy band gap under an applied transverse electric field, which has applications in optics as tunable lasers and in electronics as transistors for logical switching devices.[7–9] The latter with rotationally stacked layers exhibits properties similar to SLG.[10–12] Moreover, it shows improved charge carrier mobility.[13] Furthermore, it has been observed that the rotationally stacked BLG decouples its electronic structure and preserves the intrinsic properties of SLG. When the twist angle between the stacked layers is more than 3 degrees, the charge carrier shows the characteristics of massless Dirac fermions, but with smaller carrier velocity and when this angle exceeds 20 degrees, the layers get completely decoupled, consequently their electronic properties become indistinguishable from the SLG.[14] In recent times, for graphene growth by the CVD technique there has been worldwide interest in understanding the growth mechanism to find out the ways to control it.[15–22] The self-limiting effect of low pressure CVD growth of single layer graphene on copper vanishes when the set growth conditions are outside the optimized window and the percentage growth of SLG, BLG or FLG can vary with growth conditions.[23,24] Usually such a CVD process results in a mixture of AB stacked and twisted BLG and/or FLG. However, it remained a significant challenge to experimentally control the growth process, which yields BLG predominantly having one or other type of stacking, especially the twisted one. In light of this, in the present investigations we describe our results aimed at understanding and controlling the CVD process for the growth of BLG with exclusive rotational stacking. In order to confirm the formation of graphene and to reveal the information about layer stacking, an efficient tool, Raman spectroscopy, was employed. In thermal CVD for the growth of graphene on copper, the flux of the carbon source plays a significant role in the kinetics of graphene growth, which determines its quality and number of layers. Different geometries of the reaction site for the CVD growth of graphene were used to alter the flux of the carbon

Physics and Engineering of Carbon, Division of Materials Physics and Engineering and Academy of Scientific and Innovative Research (AcSIR)-NPL, CSIR-National Physical Laboratory (NPL), New Delhi-12, India. E-mail: kmsubhedar@gmail.com, kms@nplindia.org

source, which in turn is responsible for the number of layers and its relative orientation.

Results and discussion

In addition to the experimental conditions like the flow of reactant gases, growth pressure, temperature, *etc.*, the geometry of the reaction site has a crucial role to play in the dynamics of graphene growth. Here the reaction site is a macroscopic site where the hydrocarbon gets decomposed in the presence of a catalyst and hydrogen at reaction temperature and further growth of the graphene on the substrate surface. In order to understand the nature of layer stacking of BLG and its control with the CVD process, different sample geometries of the reaction site were explored as follows. In the first case the Cu foil was sandwiched between two quartz plates, separated by the ring shaped platinum wire spacer having a thickness more than the substrate copper foil, and was used for the graphene growth so that there exists a space between the Cu foil and quartz plate as shown in Fig. 1. The ring shape of the spacer makes an almost sealed space around the Cu foil, which helps to trap the Cu vapor flux and radicals of the carbon source during the growth. In the second case the Cu foil was kept as in the first case, but without any spacer so that the surface of the Cu foil stays intimately in contact with the quartz plate. The SEM image of the sample grown on Cu foil with this geometry is shown in Fig. 1(c). These sample geometries are referred to as 'sandwiched with wire' and 'sandwiched' geometry, respectively, and the samples grown with the above geometries are referred to as S_W and S_{Sd}, respectively.

Fig. 2(a and e) shows an optical micrograph of the graphene transferred onto the Si/SiO_2 wafer. The variation of color contrast in the optical micrograph[25] clearly indicates the BLG domain marked with a blue sketch surrounded by a single layer region as shown in Fig. 2a for the sample 'S_W'. Similarly, sample 'S_{Sd}' consisting of bilayer and single-layer regions can be easily distinguished, which are outlined by inner and outer blue sketches in Fig. 2e. Raman spectroscopy has been extensively used to characterize graphene, its quality or defect analysis, and the number of layers from characteristic peaks originating from different Raman active modes. Furthermore, it gives significant and authentic information about layer stacking in the case of BLG or FLG.[26,27] Micro-Raman mapping together with contrast imaging can be used to study the uniformity of SLG, BLG or FLG and their relative orientations. Micro-Raman mapping was performed for the S_W and S_{Sd} samples at several locations and the corresponding representative results are presented in Fig. 2. The left panel shows the (a) optical image of graphene, (b) intensity, (c) peak width ($\Delta\omega$ cm^{-1}), (d) peak position for the 2D band in Raman mapping for the graphene grown with 'sandwiched with wire' geometry and the corresponding images (e–h) in the right panel represent the 'sandwiched' sample S_{Sd}. The Raman mapping of the 2D band shows contrasting results for samples S_W and S_{Sd}. The 2D peak intensity at the central BLG region of sample S_W is considerably less compared to the surrounding SLG area with a noteworthy blue shift in its position compared to the SLG region (Fig. 2b and d). The 2D band width gets almost doubled in the central BLG region compared to the surrounded SLG region, which can be clearly seen from the color contrast in the image (Fig. 2c). All these are characteristic signatures of AB stacked BLG. For the sample

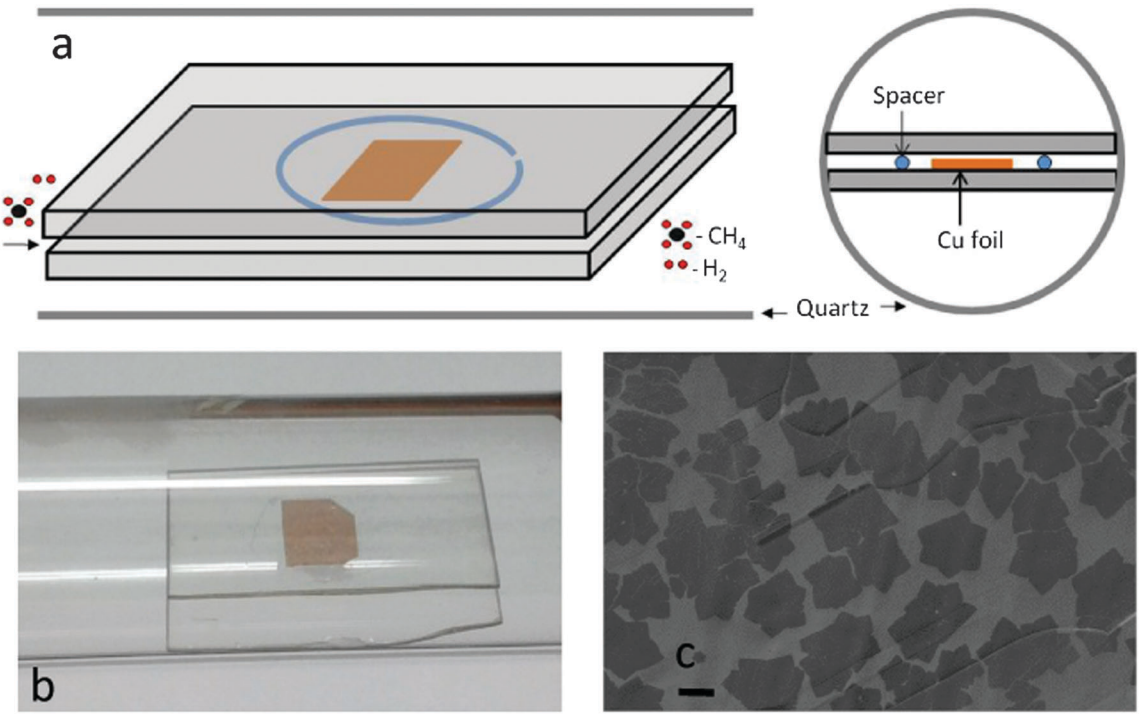

Fig. 1 (a) Schematic representing Cu foil sandwiched between two quartz plates with platinum wire as a spacer. (b) Photograph. (c) SEM image of CVD grown graphene domains on Cu foil with sandwiched geometry (scale bar – 20 μm).

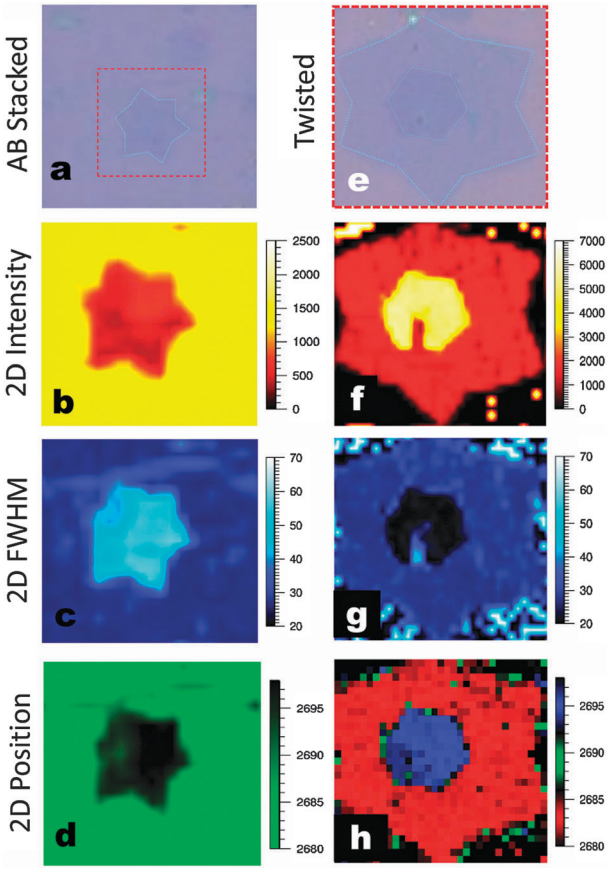

Fig. 2 2D band Raman mapping for different sample geometries. The left panel shows the corresponding (a) optical image, (b) intensity, (c) peak width FWHM ($\Delta\omega$ cm^{-1}), (d) peak position (ω cm^{-1}) for the 2D band in Raman mapping for the graphene grown with 'sandwiched with wire' geometry and the corresponding images (e–h) in the right panel show data for 'sandwiched' sample S_{Sd}. The scanned area with red dotted squares in the left panel is 20 by 20 μm and in the right panel 40 by 40 μm.

S_{Sd} with 'sandwiched' geometry, the 2D band intensity in the inner smaller BLG domain increases four times compared to the outer SLG area with a blue shift in its position, which indicates the twisted nature of BLG. However, it is surprising to see that there is no broadening of the 2D band in contrast to earlier studies.[28] In fact the 2D peak width in the BLG region remains close to the single layer values (Fig. 2g). This is due to the complete decoupling of layers with a higher twist angle.[14,29]

The shape and intensity of the 2D peak are characteristically different for SLG, AB stacked and twisted BLG. Hence, to ensure the nature of layer stacking in CVD grown BLG, the analysis of curve fitting for the 2D peak was performed. Fig. 3 shows the Raman spectra recorded at the (a) BLG domain in sample S_W, (b) single layer region and (c) bilayer region for the graphene domain in sample S_{Sd} in the left panel. The result of the curve fitting of the corresponding 2D peak for (d) AB-stacked BLG in sample S_W grown with 'sandwiched with wire' geometry (e) SLG and (f) twisted BLG with 'sandwiched' geometry is shown in the right panel. The Raman spectra recorded in the single layer region in sample S_{Sd} is typical of SLG with an I_{2D}/I_G ratio of around 3 and a narrow 2D peak having the width of around ~29, which fits with a single peak (Fig. 3b and e). However, in the case of spectra recorded in the central BLG region, the 2D peak fits with a single peak, but with a blue shift in its peak position and with a substantial increase in the I_{2D}/I_G ratio (Fig. 3c and f) because of decoupling of its electronic structure.[14,29] This clearly means that in the central BLG domain, the two layers are twisted with each other. According to the theoretical calculation and experimental data[29] the shift in the 2D peak position, intensity and FWHM of the 2D peak varies systematically with its twist angle and it remains constant after 20° *i.e.* the I_{2D} remains constant at a value double than that of the single layer, a blue shift in the 2D peak position remains at about 12 cm^{-1} and its FWHM remains at around a value close to that of the single layer. The values of these parameters in the present investigation are compared with theoretical calculations and experimental data in reference 29 and it is confirmed that the layers are twisted with each other and the angle of the twist is more than 20°. Furthermore, the optical image of sample S_{Sd} in Fig. 3, the SLG and BLG are clearly distinguished from their color contrast. Hence it is possible to calculate the angle between facets in the case of domains with a proper hexagonal shape. However, there are few domains found where it is difficult to see the facets clearly and calculate their angle exactly but still they are twisted as inferred from Raman studies. So out of ~80% twisted BLG domains, 60% domains have a twist angle of 30°(±2) and rest of the 20% domains have angles ranging between 20 and 30°. Hence, the twisted BLG growth is dominated by BLG domains with a twist angle of 30°(±2). This value of the estimated twist angle is energetically more favorable because it is the next lowest energy structure (1.6 eV per atom) with twisted stacking after the most stable AB stacking.[30]

In the case of BLG from sample S_W, the I_{2D}/I_G ratio is less than 2 and the 2D peak has a broad $\Delta\omega$ of 55 and fits with the cumulative peak having four components, each with a $\Delta\omega$ of 30, 29, 30 and 33, respectively, and the two middle peaks have higher intensities compared to the other two (Fig. 3a and d). This result is in good agreement with the fact that the 2D peak in the Raman spectra of AB stacked BLG has four components $2D_{1B}$, $2D_{1A}$, $2D_{2A}$, and $2D_{2B}$, originating from a two phonon double resonance Raman process,[31] two of which, $2D_{1A}$ and $2D_{2A}$, have higher intensities.[26] This confirms the AB stacking of the layers in BLG for sample S_W.

Raman spectra were recorded for 8–9 samples for each condition for the analysis of curve fitting and the intensity ratio to get information about layer stacking from Raman studies. For each of the sample the spectra were recorded at 4–5 different locations in the sample. Of this, 2–3 samples for each condition were studied for micro Raman measurements. About 80% of the samples for each condition show the respective layer stacking *i.e.* AB or twisted stacking as discussed above. Thus the analysis of Raman mapping and peak fitting of the 2D band unambiguously confirmed that the sample with 'sandwiched with wire' geometry results in AB stacked BLG and sample with 'sandwiched' geometry yields twisted BLG. This contrast difference in layer stacking is believed to be coming from the different kind of growth mechanism associated with different geometries. The typical low pressure CVD growth of

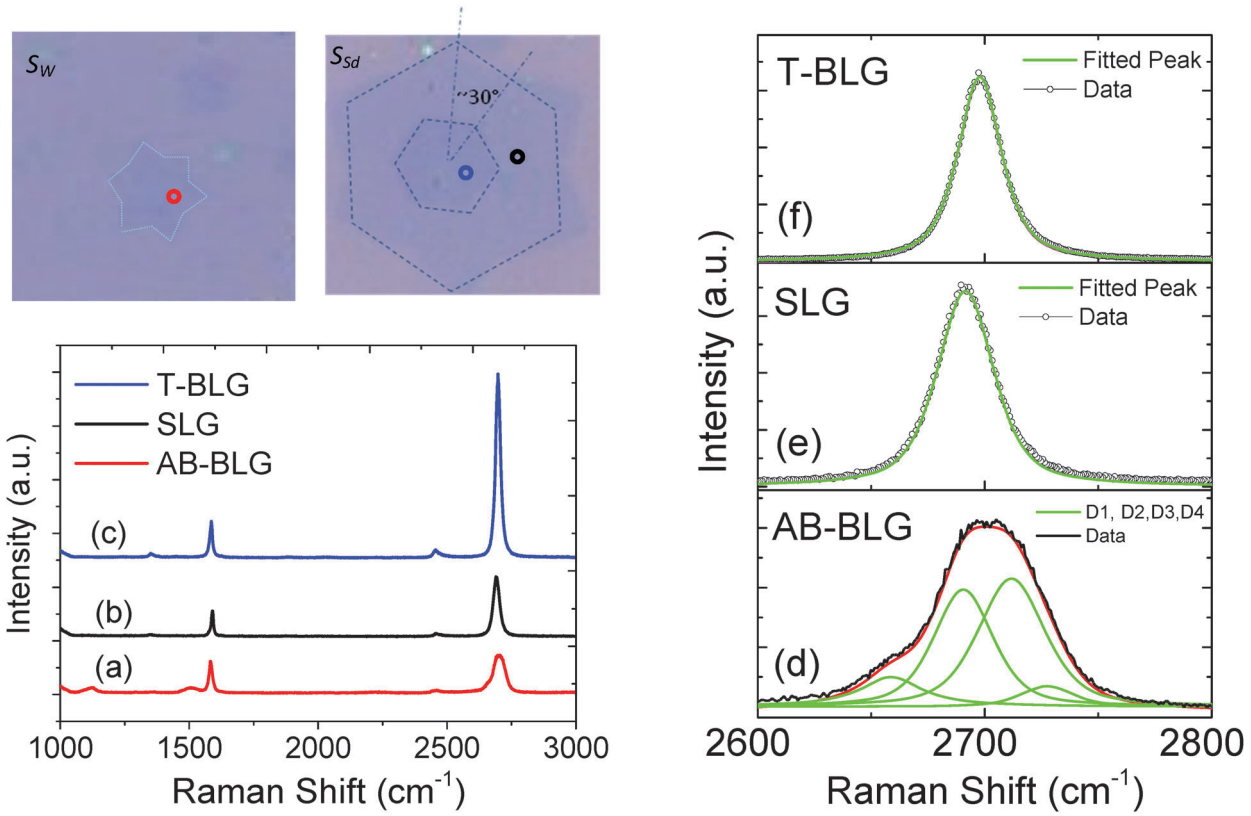

Fig. 3 Raman spectra of the (a) BLG domain in the sample S_W (b) single layer region and (c) bilayer region for the graphene sample, S_{Sd}. The curve fitting of the corresponding 2D peak for (d) AB stacked sample S_W grown with 'sandwiched with wire' geometry (e) SLG and (f) twisted BLG with 'sandwiched' geometry.

graphene on copper is a self-limiting process dominated by surface controlled growth as carbon from the catalytically cracked source covers the Cu surface, forms a monolayer and passivates the catalytic activity of the Cu surface, which inhibits further growth and the process gets restricted to the monolayer. However, this is valid only for optimum and continual supply of carbon. The enclosure geometry was introduced by Li *et al.* for the growth of large size domains.[32] The method was further used to grow the BLG and found that the growth of BLG occurs on the outside of the enclosure because of the delayed passivation of Cu from inside, leading to diffusion of carbon from the inside to outside through the Cu foil of the enclosure and the proposed mechanism based on evidence revealed it as a diffusion controlled process.[17,18] On the contrary, a different mechanism proposed again based on the evidence suggests that the growth of SLG/BLG on copper could be a surface phenomenon[15,16] or even layer by layer epitaxial growth from the top.[23] The growth process employed in these reports suggests that the sample geometry has its pronounced effect on the mechanism for the growth of BLG.

In the present case, for the sample with 'sandwiched' geometry, the Cu substrate is sandwiched between the quartz plates, where the Cu surface is intimately in contact with the quartz surface and there is no direct flow of reactant gas over the Cu surface. However, as illustrated by the mechanism in Fig. 4, the gases can leak in between the Cu surface and quartz surface with a very slow rate, which reduces the supply of the carbon source creating a quasi-static distribution of reactant gases, which causes delay in surface coverage of Cu with monolayer graphene. Subsequently, with time carbon gets diffused through bulk of the Cu foil and reaches the other side of the foil, where it grows as a second layer underneath the top layer and forms the BLG similar to the enclosure growth method,[17] but with a significant difference that here, the Cu foil is sandwiched between the two quartz plates, causing the BLG to grow exclusively under diffusion control because neither of the Cu side is directly exposed to the flow of the gases. This is very important as all the BLGs grown will have a similar kind of growth environment and process. Furthermore, adding a

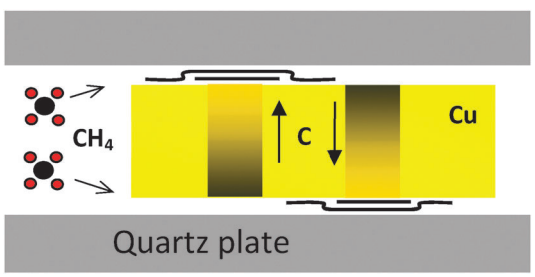

Fig. 4 Schematic illustrating the growth mechanism of BLG with 'sandwiched' geometry.

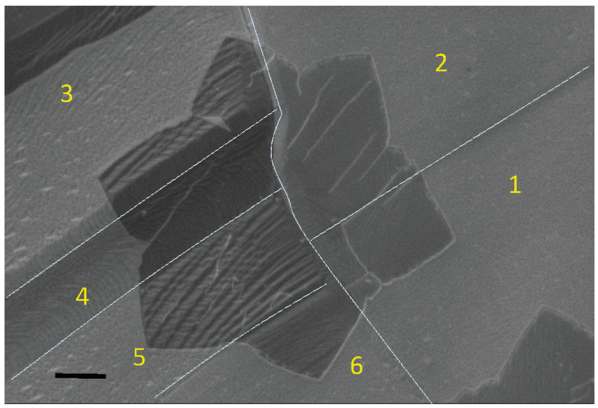

Fig. 5 SEM of the graphene domain grown across different facets and grain boundary of Cu (scale bar – 5 μm).

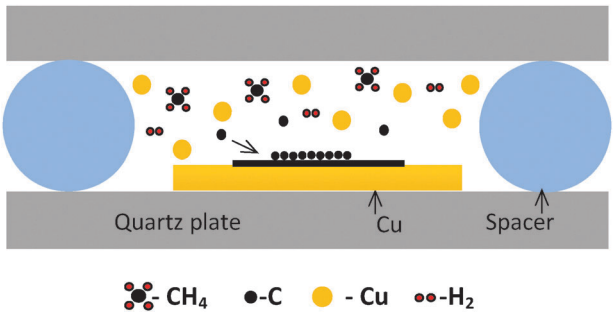

Fig. 6 Schematic illustrating the growth mechanism of BLG with 'sandwiched with wire' geometry.

second layer from beneath requires debonding of the first layer; the weak interaction between Cu and graphene favors this debonding.[33] The weak nature of this interaction can be inferred from observation of graphene domains growing without impediment across facets and copper grain boundaries as shown in Fig. 5 and from theoretical work that found a weak electronic interaction between graphene and Cu, manifested by preservation of the Dirac cones.[34] It was also reported that the growth of the second layer from below prefers the first layer, which is rotated with respect to the substrate orientation because of its weak bonding.[35] This kind of graphene growth of the second layer on the copper has many rotational variants because of its weak interactions with Cu. Neither the substrate nor the overlying graphene strongly locks the underneath second layer in the same orientation as the overlying first graphene layer, leading to BLG with twisted stacking.[36] Hence, the twisted layer stacking of BLG in our sample with sandwiched geometry is originating from an exclusive diffusion controlled process under quasi-static control and weak interactions of graphene with Cu.

In the case of 'sandwiched with wire' geometry because of the spacer, the Cu surface is not intimately in contact with the quartz surface. Hence, the reactant gases can enter relatively easily inside the closed space formed because of the spacer, where the extra carbon radicals or fragments generated from methane in the presence of trapped Cu vapor flux[37] inside the closed space get adsorbed on monolayer graphene, which usually get covered in an initial short time. The proposed mechanism is illustrated in Fig. 6. This could lead to the growth of second layer graphene from the top on the fast grown first layer. Consequently, the growth of BLG is dominated by AB stacking and the underlying mechanism could be the surface controlled growth. It is reasonable to accept this growth mechanism as it is consistent with the earlier reports, where they adopted a similar kind of approach to grow the second layer epitaxially from the top on already grown monolayer graphene with the aid of an additional fresh Cu foil as a catalyst to create an extra carbon flux for the growth of the second layer.[23,24]

The contrast nature of layer stacking for samples with different geometries of the reaction site suggests its different underlying growth mechanisms, originating from the process which supplies the extra carbon flux, needed for the growth of second layer *i.e.* by diffusion through Cu foil or from the top in the presence of Cu vapor flux. The different geometries of the reaction site indicate the nature of the BLG growth process, which is either dominated by the diffusion controlled or surface controlled mechanism, which in turn is responsible for different layer stacking of BLG.

The CVD process employed in the present investigations yields samples with good uniformity. The size of the Cu foil or substrate used for the CVD growth is 20 × 20 mm and the growth is consistently uniform all over the substrate except at edges where at about 1 mm there is non-uniform growth and uncovered regions were observed. Furthermore, large area samples can be grown using the CVD system with a quartz reactor of a larger diameter. In the case of 'sandwiched with wire' growth for AB stacked BLG, the trapping of the Cu vapor is very crucial. It will help to supply source carbon even after the coverage of single layer graphene. The appropriate diameter of the spacer wire for efficient trapping of Cu vapors, flow rate of the reactant gases and temperature are crucial parameters needed to tune to get good yield.

Samples S_W and S_{Sd} sometimes in contrast results in twisted and AB stacked BLG, respectively, which are very rare. At some places occasionally graphene grows by more than two layers. Overall the S_W geometry is dominated by AB stacked and S_{Sd} geometry is dominated by twisted BLG.

Conclusions

Different geometries of the reaction site for the growth of BLG and their effect on the nature of layer stacking are demonstrated. Raman mapping and curve fitting analysis confirmed the type of layer stacking for the BLG grown by the CVD technique. The sample grown with a sandwiched structure such as quartz/Cu foil/quartz along with a spacer, between the two quartz plates to create a sealed space, resulted in AB stacked BLG, while the sandwiched geometry without a spacer yields samples with twisted BLG. This contrast difference in layer stacking is a consequence of the difference in the growth mechanism associated with different geometries of the reaction site. The diffusion dominated process under quasi-static control created with the aid of the sandwiched structure leads to the growth of twisted BLG

while surface controlled growth with ample and continual supply of carbon created with the aid of the sandwiched structure with a spacer leads to AB stacked BLG. Through this new approach, an efficient technique to control the layer stacking of BLG grown by CVD is presented, which can be used to tailor its electronic properties. The present study will advance the understanding of stacking control in graphene growth with CVD, which is important for technological applications that rely either on energy gap and high carrier mobility of the graphene, like electronic switching devices or graphene r.f. transistors. This will allow for a more efficient engineering of bilayer graphene. Junctions between twisted and Bernal-stacked BLG could also enable novel heterostructure devices.

Experimental section

Prior to graphene growth, 25 μm thick copper foil (99.8% Cu, Alfa Aesar #13382) was thoroughly cleaned with acetone, acetic acid, DI water and IPA. The copper foil was placed inside a quartz reactor at an isothermal zone of a custom built thermal CVD system and evacuated, filled with argon and again pumped down to 0.005 mbar, then heated to 1045 °C under hydrogen flow of 12 sccm. Hydrogen flow was reduced to 8 sccm and kept for annealing for 20 min to increase grain growth/crystallinity of the Cu foil and remove the thin oxide layer grown on it. Subsequently, for the growth of graphene methane was introduced with a flow rate of 4 sccm for an initial time period of 3 minutes followed by an increase in its flow rate to 25 sccm with a total growth time of 30 minutes. After growth the samples were cooled down quickly by sliding the furnace. Methane flow was turned off at 650 °C and hydrogen below 100 °C. The pressure inside the CVD reactor during the growth was about 0.130 and 0.4 mbar, respectively, for the first 3 min and the rest of the growth. In order to transfer the CVD grown graphene on silicon wafer, PMMA solution (molecular weight 495 000 g mol^{-1}, 4% by volume dissolved in anisole) was spin coated onto the top side of the sample at 3000 rpm and dried overnight, subsequently, was put in 20% ammonium persulphate (APS) etchant solution in deionized water as a copper etchant for two hours followed by additional etching with a fresh etchant for 12 hours to ensure the complete etching of copper. After the etching step the PMMA supported graphene was rinsed with deionized water several times before scooping out with the substrate. The PMMA was finally removed with warm acetone. The silicon substrates used in this work were highly p-doped and with 300 nm thermal oxide on the top. The micro-Raman mapping was performed under ambient conditions using a Renishaw InVia micro-Raman spectrometer equipped with a 514 nm (2.41 eV) wavelength excitation laser and 2400 lines per mm grating. A laser beam size of ~1 μm with a ×50 objective lens is used.

Acknowledgements

Authors are thankful to Director, CSIR-NPL, for his permission to publish the results. This research has been supported by the Council of Scientific and Industrial Research (CSIR). One of the authors IS would like to thank CSIR for granting Senior Research fellowship.

References

1 K. S. Novoselov, A. K. Geim, S. V. Morozov, D. Jiang, Y. Zhang, S. V. Dubonos, I. V. Grigorieva and A. A. Firsov, *Science*, 2004, **306**, 666.
2 K. S. Novoselov, A. K. Geim, S. V. Morozov, D. Jiang, M. I. Katsnelson, I. V. Grigorieva, S. V. Dubonos and A. A. Firsov, *Nature*, 2005, **438**, 197.
3 A. K. Geim and K. S. Novoselov, *Nat. Mater.*, 2007, **6**, 183.
4 Z. G. Fthenakis and N. N. Lathiotakis, *Phys. Chem. Chem. Phys.*, 2015, **17**, 16418.
5 W. Yong, Z. Xue-Qing and L. Hui, *Chin. Phys. Lett.*, 2014, **31**, 117201.
6 X. S. Li, W. W. Cai, J. H. An, S. Kim, J. Nah, D. X. Yang, R. Piner, A. Velamakanni, I. Jung, E. Tutuc, S. K. Banerjee, L. Colombo and R. S. Ruoff, *Science*, 2009, **324**, 1312.
7 C. H. Lui, Z. Li, K. F. Mak, E. Cappelluti and T. F. Heinz, *Nat. Phys.*, 2011, **7**, 944.
8 E. Castro, K. Novoselov, S. Morozov, N. Peres, J. dos Santos, J. Nilsson, F. Guinea, A. Geim and A. Neto, *Phys. Rev. Lett.*, 2007, **99**, 216802.
9 Y. Zhang, T. T. Tang, C. Girit, Z. Hao, M. C. Martin, A. Zettl, M. F. Crommie, Y. R. Shen and F. Wang, *Nature*, 2009, **459**, 820.
10 J. Hass, F. Varchon, J. E. Millán-Otoya, M. Sprinkle, N. Sharma, W. A. de Heer, C. Berger, P. N. First, L. Magaud and E. H. Conrad, *Phys. Rev. Lett.*, 2008, **100**, 125504.
11 J. M. B. Lopes dos Santos, N. M. R. Peres and A. H. Castro, *Phys. Rev. Lett.*, 2007, **99**, 256802.
12 M. Sprinkle, D. Siegel, Y. Hu, J. Hicks, A. Tejeda, A. Taleb-Ibrahimi, P. Le Fèvre, F. Bertran, S. Vizzini, H. Enriquez, S. Chiang, P. Soukiassian, C. Berger, W. A. de Heer, A. Lanzara and E. H. Conrad, *Phys. Rev. Lett.*, 2009, **103**, 226803.
13 B. Dlubak, M.-B. Martin, C. Deranlot, B. Servet, S. Xavier, R. Mattana, M. Sprinkle, C. Berger, W. A. De Heer, F. Petroff, A. Anane, P. Seneor and A. Fert, *Nat. Phys.*, 2012, **8**, 557.
14 A. Luican, G. H. Li, A. Reina, J. Kong, R. R. Nair, K. S. Novoselov, A. K. Geim and E. Y. Andrei, *Phys. Rev. Lett.*, 2011, **106**, 126802.
15 X. Li, W. Cai, L. Colombo and R. S. Ruoff, *Nano Lett.*, 2009, **9**, 4268.
16 X. Li, C. W. Magnuson, A. Venugopal, J. An, J. W. Suk, B. Han, M. Borysiak, W. Cai, A. Velamakanni, Y. Zhu, L. Fu, E. M. Vogel, E. Voelkl, L. Colombo and R. S. Ruoff, *Nano Lett.*, 2010, **10**, 4328.
17 W. J. Fang, A. L. Hsu, Y. Song, A. G. Birdwell, M. Amani, M. Dubey, M. S. Dresselhaus, T. Palacios, J. Kong and J. Kong, *ACS Nano*, 2014, **8**, 6491.
18 W. Fang, A. L. Hsu, R. Caudillo, Y. Song, A. G. Birdwell, E. Zakar, M. Kalbac, M. Dubey, T. Palacios and M. S. Dresselhaus, *Nano Lett.*, 2013, **13**, 1541.
19 S. Bhaviripudi, X. Jia, M. S. Dresselhaus and J. Kong, *Nano Lett.*, 2010, **10**, 4128.

20 I. Vlassiouk, M. Regmi, P. Fulvio, S. Dai, P. Datskos, G. Eres and S. Smirnov, *ACS Nano*, 2011, **5**, 6069.
21 B. Wu, D. Geng, Z. Xu, Y. Guo, L. Huang, Y. Xue, J. Chen, G. Yu and Y. Liu, *NPG Asia Mater.*, 2013, **5**, e36.
22 Y. Li, M. Li, T. Wang, F. Bai and Y.-X. Yu, *Phys. Chem. Chem. Phys.*, 2014, **16**, 5213.
23 K. Yan, H. Peng, Y. Zhou, H. Li and Z. Liu, *Nano Lett.*, 2011, **11**, 1106.
24 L. Liu, H. Zhou, R. Cheng, W. J. Yu, Y. Liu, Y. Chen, J. Shaw, X. Zhong, Y. Huang and X. Duan, *ACS Nano*, 2012, **6**, 8241.
25 P. Blake, E. W. Hill, A. H. C. Neto, K. S. Novoselov, D. Jiang, R. Yang, T. J. Booth and A. K. Geim, *Appl. Phys. Lett.*, 2007, **91**, 063124.
26 A. C. Ferrari, J. C. Meyer, V. Scardaci, C. Casiraghi, M. Lazzeri, F. Mauri, S. Piscanec, D. Jiang, K. S. Novoselov, S. Roth and A. K. Geim, *Phys. Rev. Lett.*, 2006, **97**, 187401.
27 P. Poncharal, A. Ayari, T. Michel and J. L. Sauvajol, *Phys. Rev. B: Condens. Matter Mater. Phys.*, 2008, **78**, 113407.
28 P. Lespade and A. Marchand, *Carbon*, 1984, **22**, 375; Cross reference from A. C. Ferrari and D. M. Basko, *Nat. Nanotechnol.*, 2013, **8**, 235.
29 K. Kim, S. Coh, L. Z. Tan, W. Regan, J. M. Yuk, E. Chatterjee, M. F. Crommie, M. L. Cohen, S. G. Louie and A. Zettl, *Phys. Rev. Lett.*, 2012, **108**, 246103.
30 S. Shallcross, S. Sharma and O. A. Pankratov, *J. Phys.: Condens. Matter*, 2008, **20**, 454224.
31 C. Thomsen and S. Reich, *Phys. Rev. Lett.*, 2000, **85**, 5214.
32 X. S. Li, C. W. Magnuson, A. Venugopal, R. M. Tromp, J. B. Hannon, E. M. Vogel, L. Colombo and R. S. Ruoff, *J. Am. Chem. Soc.*, 2011, **133**, 2816.
33 H. Chen, W. G. Zhu and Z. Y. Zhang, *Phys. Rev. Lett.*, 2010, **104**, 186101.
34 P. A. Khomyakov, G. Giovannetti, P. C. Rusu, G. Brocks, J. van den Brink and P. J. Kelly, *Phys. Rev. B: Condens. Matter Mater. Phys.*, 2009, **79**, 195425.
35 S. Nie, A. L. Walter, N. C. Bartelt, E. Starodub, A. Bostwick, E. Rotenberg and K. F. McCarty, *ACS Nano*, 2011, **5**, 2298.
36 S. Nie, W. Wu, S. Xing, Q. Yu, J. Bao, S. Pei and K. F. McCarty, *New J. Phys.*, 2012, **14**, 093028.
37 H.-C. Lin, Y.-Z. Chen, Y.-C. Wang and Y.-L. Chueh, *J. Phys. Chem. C*, 2015, **119**, 6835.

